Accepted Manuscript

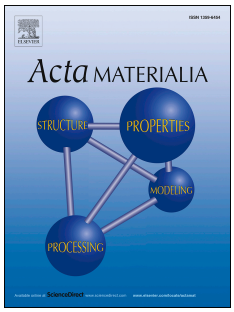

Dramatically reduced lattice thermal conductivity of Mg_2Si thermoelectric material from nanotwinning

Guodong Li, Jiangang He, Qi An, Sergey I. Morozov, Shiqiang Hao, Pengcheng Zhai, Qingjie Zhang, William A. Goddard, III, G. Jeffrey Snyder

PII: S1359-6454(19)30127-2

DOI: https://doi.org/10.1016/j.actamat.2019.02.041

Reference: AM 15164

To appear in: *Acta Materialia*

Received Date: 12 February 2019

Revised Date: 25 February 2019

Accepted Date: 25 February 2019

Please cite this article as: G. Li, J. He, Q. An, S.I. Morozov, S. Hao, P. Zhai, Q. Zhang, W.A. Goddard III., G.J. Snyder, Dramatically reduced lattice thermal conductivity of Mg_2Si thermoelectric material from nanotwinning, *Acta Materialia*, https://doi.org/10.1016/j.actamat.2019.02.041.

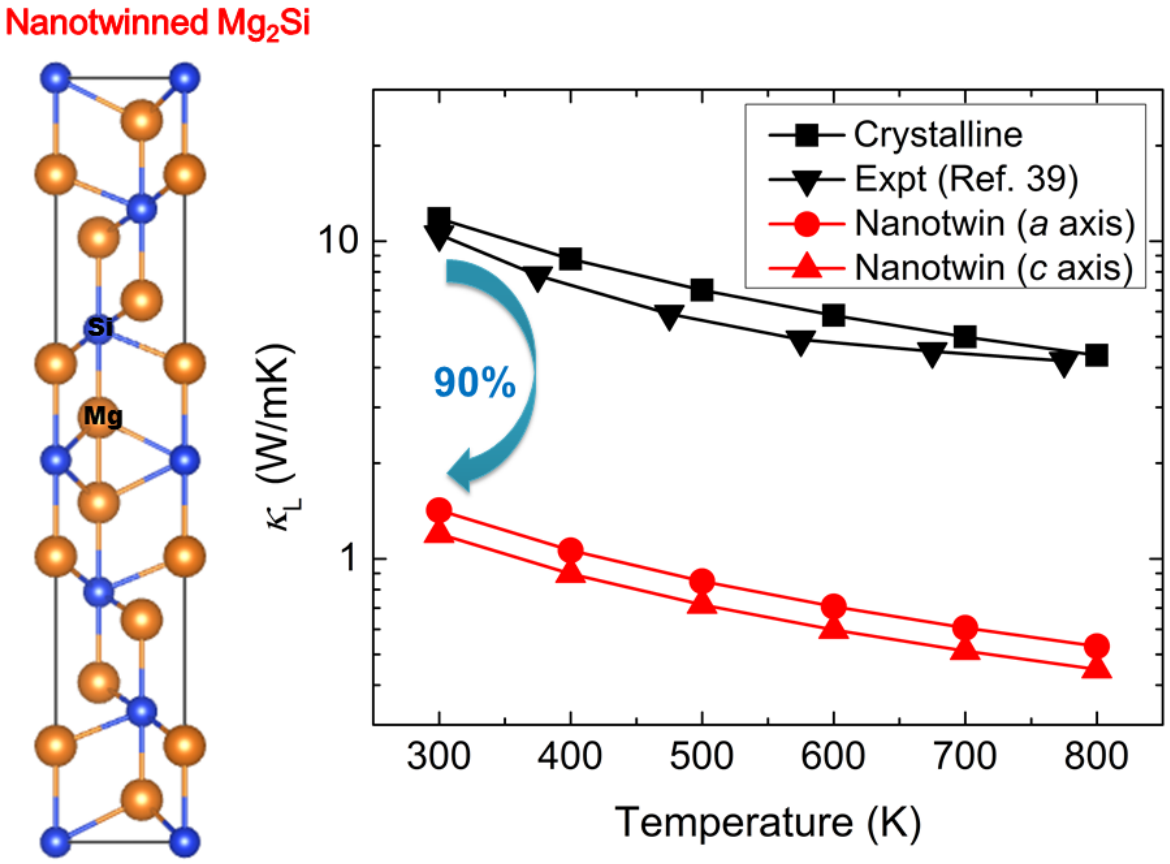
Nanotwinned Mg_2Si
Si
Mg
κ_L (W/mK)
10
1
90%
Crystalline
Expt (Ref. 39)
Nanotwin (*a* axis)
Nanotwin (*c* axis)
300
400
500
600
700
800
Temperature (K)

Dramatically reduced lattice thermal conductivity of Mg_2Si thermoelectric material from nanotwinning

Guodong Li [a,b], Jiangang He [b], Qi An [c], Sergey I. Morozov [d], Shiqiang Hao [b], Pengcheng Zhai [*,a], Qingjie Zhang [a], William A. Goddard III [e], and G. Jeffrey Snyder [*,b]

[a]Hubei Key Laboratory of Theory and Application of Advanced Materials Mechanics, School of Science, Wuhan University of Technology, Wuhan 430070, China.

[b]Department of Materials Science and Engineering, Northwestern University, Evanston, Illinois 60208, USA.

[c]Department of Chemical and Materials Engineering, University of Nevada Reno, Reno, Nevada 89557, USA

[d]Department of Computer Simulation and Nanotechnology, South Ural State University, Chelyabinsk 454080, Russia

[e]Materials and Process Simulation Center, California Institute of Technology, Pasadena, California 91125, USA.

[*]Corresponding authors: pczhai@126.com; jeff.snyder@northwestern.edu

Abstract: Tuning phonon transport to reduce the lattice thermal conductivity (κ_L) is crucial for advancing thermoelectrics (TEs). Traditional strategies on κ_L reduction focus on introducing scattering sources such as point defects, dislocations, and grain boundaries, that may degrade the electrical conductivity and Seebeck coefficient. We suggest here, a novel twin boundary (TB) strategy that can decrease the κ_L of Mg_2Si by ~90%, but which may not degrade the electrical properties significantly. We validate this suggestion using density functional theory (DFT). We attribute the mechanism of TB induced κ_L reduction to (i) the lower phonon velocities and larger Grüneisen parameter, (ii) "rattling" of the Mg–Mg pair induced soft acoustic and optical modes, (iii) shorter phonon lifetime and higher phonon scattering rate. We predict that the size of nanotwinned structure should be controlled between 3 nm and 100 nm in the Mg_2Si matrix for the most effective κ_L reduction. These results should be applicable for other TE or non TE energy materials with desired low thermal conductivity, suggesting rational designs of high-performance Mg_2Si TE materials with low κ_L for the energy conversion applications.

Keywords: Mg_2Si Thermoelectric Material; Thermal Conductivity; Nanotwinning; Density Functional Theory

1. INTRODUCTION

Since the 20th century, overconsumption of fuel oils and the resulting energy crisis has been increasingly causing such environmental issues as global climate change, acid rain pollution, and marine pollution. Solid-state thermoelectric (TE) technology, enabling direct conversion between heat and electricity without moving parts, offers the possibility for relieving the current energy crisis [1,2]. The widespread application of TE technology requires TE materials with high conversion efficiency, which is characterized by the materials' dimensionless figure of merit zT, $zT = S^2\sigma T/(\kappa_E+\kappa_L)$, where S, σ, κ_E, κ_L, and T are the Seebeck coefficient, electrical conductivity, electronic thermal conductivity, lattice thermal conductivity and absolute temperature, respectively [1-5]. To achieve a high zT value, TE materials should have a high Seebeck coefficient, a high electrical conductivity, and a low total (electronic and lattice) thermal conductivity.

The current strategies for enhancing the zT value are mainly focused either on improving the power factor ($S^2\sigma$) by tailoring the electrical transport properties [6,7] or on reducing κ_L through phonon scattering [8-11]. Due to the strong correlation between S, σ, and κ_E, traditional strategy of carrier optimization is often not very effective in improving zT [1,12,13]. Two decades ago, Dresselhaus *et al.* proposed a concept of quantum confinement for effectively decoupling the correlation between S, σ, and κ_E [14,15]. Then, various effective band modification approaches (such as band convergence [16-18], distortion [19], and nestification [20].) were developed to decouple these three parameters and enhance the $S^2\sigma$ and zT. Alternatively, exploring effective reduction strategies for κ_L (the only independent parameter) or seeking low κ_L materials has consistently led to advances in high-performance TE materials [21-26]. For example, the extraordinary 'liquid-like' behavior in $Cu_{2-x}Se$ results in an intrinsically low κ_L of $0.4\,W\,m^{-1}\,K^{-1}$ and a zT of 1.5 at 1000 K [21]. In SnSe single crystals, The lattice anharmonicity leads to an exceptionally low κ_L of $0.23 \pm 0.03\,W\,m^{-1}\,K^{-1}$ and an unprecedented zT of 2.6 ± 0.03 at 923 K [22,23]. In such TE materials as MgAgSb [24], $Ag_{5-\delta}Te_3$ [25], and Ag_8SnSe_6 [26], the complex crystal structure or weak chemical bonds leads to low heat capacity or low speed of sound, well explaining the low intrinsic κ_L of $< 0.5\,W\,m^{-1}\,K$ [24-26]. Introducing phonon scattering sources such as point defects [27-29], dislocations [30-32], grain boundaries [33-35], can effectively shorten phonon relaxation time, giving rise to reduction in κ_L. Multiple fillers in $CoSb_3$ can achieve broad-frequency phonon scattering, reducing κ_L to the glass limit value of $0.2\,W\,m^{-1}\,K^{-1}$, and leading to an extremely high zT of 1.7 at 850 K [29]. Full-spectrum phonon scattering, which was achieved through grain boundary, dense dislocation arrays, and point defect,

leads to a substantially lower κ_L of 0.33 $W m^{-1} K^{-1}$ and a dramatic high zT of 1.86 at 320 K in $Bi_{0.5}Sb_{1.5}Te_3$ bulk alloys [30].

Twin boundaries (TBs), a thermodynamically stable planar defect, could provide another phonon scattering source to effectively suppress κ_L [36-38]. Ren. *et al.* prepared nanotwinned InSb and found that phonons can be scattered by TBs [36]. Shin. *et al.* found TB induced crystal defect reduced κ_L from 1.9 to 1.4 $W m^{-1} K^{-1}$ for twin-contained Bi_2Te_3 nanowires [37]. Zhou *et al.* found that nanotwins in PbTe can effectively reduce κ_L [38]. These findings suggest that TBs play significant roles in phonon scattering and κ_L reduction without degrading electronic transport properties. However, the determining factors for TB induced κ_L reduction and the underlying scattering mechanisms remain unexplored.

To understand the role of TB on κ_L and the underlying phonon scattering mechanism, we carried out DFT phonon calculations and solved the linearized Boltzmann equation to examine the phonon transport properties of single crystalline and nanotwinned Mg_2Si. We find that TB can reduce κ_L by ~ 90%, as shown in Fig. 1. At 300 K, the κ_L of nanotwinned Mg_2Si is 1.42 and 1.20 $W m^{-1} K^{-1}$ along the *a* and *c* axis, respectively, only ~10% of that (11.8 $W m^{-1} K^{-1}$) in single crystalline Mg_2Si. We attribute this remarkable κ_L reduction to the following three mechanisms: (i) lower phonon velocities and larger Grüneisen parameter, (ii) "rattling" of the Mg–Mg pair induced soft acoustic and optical modes, (iii) shorter phonon lifetime and higher phonon scattering rate in nanotwinned Mg_2Si.

The density of nanotwins is closed related to the various properties of nanotwins. Studying how density of nanotwins influences the κ_L requires large-scale atomic simulations such as molecular dynamics. This will be considered as a future study.

2. METHODOLOGY

All density functional theory (DFT) calculations were performed within the VASP code using the projector augmented wave (PAW) method [40-42]. The Perdew-Burke-Ernzerhof (PBE) version of the generalized gradient approximation (GGA) was adopted to describe the exchange correlation interaction [43].

Γ-centered symmetry reduced Monkhorst-Pack meshes with a fine resolution of $2\pi \times 1/40$ $Å^{-1}$ were used to sample the *k*-points in the first Brillouin zone. An energy cutoff of 500 eV was used for the plane-wave expansion, with the electronic energy and force convergence criteria of 1×10^{-6} eV and 1×10^{-2} eV/Å, respectively.

Phonon dispersion calculations were carried out with the PHONOPY package using the frozen phonon method [44]. The 3×3×3 supercell (81 atoms) for flawless Mg_2Si and 3×3×1 supercell (162 atoms) for nanotwinned Mg_2Si were chosen for the second order force constant calculations. The third order force constants of the flawless and nanotwinned Mg_2Si were computed using the thirdorder.py code with 3×3×3 and 2×2×1 supercells [45]. The phonon lifetime, scattering rate, and κ_L were carried out within the ShengBTE code by solving the Boltzmann transport equation [46].

3. RESULTS AND DISCUSSION

Mg_2Si crystalizes in a face centered cubic (FCC) structure with space group $Fm\bar{3}m$ (225). The unit cell contains 8 × Mg and 4 × Si atoms with Mg occupying the (1/4, 1/4, 1/4) site and Si occupying the (0, 0, 0) site (Fig. 2(a)). Each Mg atom is tetrahedrally coordinated to Si atoms with a Mg–Si bond length of 2.75 Å. The shared electron localization function (ELF) isosurfaces between Mg and Si atoms imply covalent character of the Mg–Si bond (Fig. 2(b)). Our optimized lattice parameter is a = 6.359 Å, only 0.1% larger than the experimental value of 6.351 Å at room temperature [47].

Previous experimental results showed that the most stable coherent twin of Mg_2Si is the deformation twin with TBs along the {1-1-1} plane [48]. Here, we utilized DFT to relax the initial nanotwinned Mg_2Si and then determined the stable atomic geometry, leading to the structure shown in Fig. 2(c). The nanotwinned structure contains 24× Mg and 12 × Si atoms with lattice parameters a = 7.74 Å, b = 4.47 Å, c = 22.94 Å, $\alpha = \beta = \gamma = 90^\circ$ (Fig. 2(c)) This leads to a hexagonal primitive cell containing 12× Mg and 6 × Si atoms, as shown in Fig. S1 in the Supporting Material. The twin spacing is 1.15 nm with Si atoms sitting in the TB. Within the TB, two Mg–Mg bonds form, coupling the upper and lower half of the twinned structure. This Mg–Mg length (2.55 Å) is shorter than the covalent bond length (2.85 Å) [50] and much shorter than the metallic bond (3.20 Å) [51], implying covalent character for the Mg–Mg interaction in the TB. The Mg–Si bond length in the TBs is 2.88 Å, which is 0.13 Å longer than that (2.75 Å) in single crystalline Mg_2Si. This leads to a much weaker Mg–Si bond in the TBs than that in the Mg_2Si crystal. The upper half of the nanotwinned Mg_2Si is the (1-1-1)[1-12] slip system, while the lower half is (1-1-1)[-11-2]. Our previous DFT simulations suggested that the (1-1-1)[-11-2] slip system is the most likely under pressure [49]. These results explain why the shear stress induced during the synthetic processing can generate this deformation twin experimentally [48].

An inherently low κ_L generally arises from low phonon velocities (v_s) and larger Grüneisen parameters (γ_G). We first calculated the v_s, extracted from the slope of phonon dispersion around Γ point (Fig. 3). As listed in Table. 1, we calculate that v_s = 3915 m/s for nanotwinned Mg_2Si to be 13% lower than that (4427 m/s) of single crystalline Mg_2Si. This decrease is probably because the TB leads to a bond length (2.88 Å) 4.7% longer than that in the flawless crystal (Fig. 2). This weaker Mg–Si bonding interaction leads to a softer structural rigidity, resulting in lower v_s in the nanotwinned structure. To determine the structural stability of flawless and nanotwinned Mg_2Si, We calculated the elastic matrix elements (See Table S1 in the SM) and used the Voigt-Reuss-Hill relationship to calculate the *B* and *G* (Table. 1) [52]. We found that *G* = 32.4 GPa in nanotwinned Mg_2Si is significantly lower (36%) than that (50.6 GPa) in the flawless crystal. This indicates that the global structural rigidity of nanotwinned Mg_2Si is weaker than that in flawless Mg_2Si, even though a covalent Mg–Mg bond forms in the nanotwinned structure. This provides another explanation of why the v_s in nanotwinned Mg_2Si is lower than that in its flawless crystal.

The Grüneisen parameter (γ_G) characterizes the strength of lattice anharmonicity, providing another intrinsic material parameter related to the physical nature of thermal transport behavior. The γ_G of flawless Mg_2Si is 1.38 (Table 1), which is higher than that of single crystalline $CoSb_3$ (0.92) [53]. This explains why flawless Mg_2Si with simple unit cell, light elements and large phonon velocity (4427 m/s) possesses a comparable κ_L (11.8 W/mK at room temperature) with single crystalline $CoSb_3$ (10 W/mK) [53]. The calculated γ_G of nanotwinned Mg_2Si is 1.49 (Table 1), higher than that of flawless Mg_2Si. The larger γ_G reflects a higher lattice anharmonicity in the nanotwinned Mg_2Si. As the nanotwinned Mg_2Si is mechanically sheared, the antisymmetric deformation of upper and lower half part leads to the distorted TB [49]. While the Mg-Si framework uniformly resists the deformation in flawless Mg_2Si [49]. Because of the weaker Mg–Si bond in the TB discussed above, the TB rigidity is much softer than the Mg-Si framework. This explains why the nanotwinned Mg_2Si exhibits a larger anharmonicity than the flawless crystal.

To determine the underlying mechanism of the extremely low κ_L for nanotwinned Mg_2Si, we investigated the phonon dispersion along the high-symmetry directions and the phonon density of states (PDOS) of single crystalline and nanotwinned Mg_2Si, as shown in Fig. 3. We highlighted the acoustic modes with different colors because they are expected to play significant roles in the thermal transport. For frequencies less than 125 cm^{-1}, the Mg and Si atom in flawless Mg_2Si contribute equally to acoustic phonon branches (Fig. 3(c)). However, at high frequencies (>125 cm^{-1}), the longitudinal acoustic (LA) phonon branches strongly overlap with the optical phonon modes along the Γ – X and Γ – K directions (Fig. 2(b)). We attribute these behaviors to the

similar atom masses between Mg and Si elements. Avoided crossings between the LA and optical branches along the Γ – K and Γ – L directions lead to suddenly decreased LA phonon energy. This softening of the phonon mode arises from avoided crossings, providing another reason why flawless Mg_2Si possesses an κ_L comparable with $CoSb_3$ [53]. In nanotwinned Mg_2Si, we observed similar avoided crossings along the Γ – M and Γ – K directions, leading to flat LA phonon dispersions with a maximum frequency of 115 cm^{-1}. This value is much lower than the maximum LA phonon frequency (288 cm^{-1}) in flawless Mg_2Si. As shown in Fig. 3(e), the transverse acoustic (TA') phonons in nanotwinned Mg_2Si are also flat and soft. The avoided crossings induced acoustic phonon softening similar to that found in other low κ_L TE compound such as full-Heusler Ba_2AuBi [54] and filled $CoSb_3$ [55]. Thus, we attribute the origin of low κ_L to the atomic rattling in these compounds. Analogously to clathrates, we attributed the flat and soft acoustic modes to the Mg–Mg pair "rattling" in the TB (Fig. 3(f)). The Mg1 atoms in the TB are linked with each other with a strong Mg–Mg covalent bond of 2.55 Å (Fig. 2(b) and Fig. 3(f)), but the Mg1 interacts more weakly with the Si1 atom with the longer Mg–Si bond of 2.88 Å (Fig. 2(b) and Fig. 3(f)). Thus we suggest that the Mg–Mg pair behaves as a rattling center that scatters heat-carrying phonons, similar to the guest atom in clathrate $CoSb_3$. This is consistent to the PDOS (Fig. 3(f)), which shows clearly that the Mg1 atom in the TB dominates the contribution of low energy phonons (65 to 115 cm^{-1}). In addition, the lattice distortion caused by the Mg–Mg pair also leads to low frequency optical phonons. The lowest optical phonon is only 25 cm^{-1} at **A** point (Fig. 3(e)). This value is much lower than that of flawless Mg_2Si (145 cm^{-1}), and even lower than that of other low κ_L TE compounds, such as filled $CoSb_3$ (42 cm^{-1}) [55]. These soft acoustic and optical phonons in nanotwinned Mg_2Si demonstrate the "rattling" of the Mg–Mg pair as a mechanism by which the TB lowers κ_L of Mg_2Si.

To further understand the role of TBs on thermal transport, we calculated the phonon lifetime as a function of frequency for nanotwinned and flawless Mg_2Si at room temperature, as shown in Fig. 4. The phonon lifetimes show the general trend that low frequency acoustic phonons have longer lifetimes than high frequency optical phonons [56]. We find that the phonon lifetimes of nanotwinned Mg_2Si are much shorter than those of flawless Mg_2Si. This indicates much stronger scattering in nanotwinned Mg_2Si, which we attribute mainly to resonant scattering caused by the Mg–Mg pair "rattling" in the TB. In nanotwinned Mg_2Si, acoustic phonon lifetimes show a dip at the frequency of 82 cm^{-1} and 115 cm^{-1} which corresponds to the flat LA and TA' phonons as shown in Fig. 3(e). This is another indication that soft LA and TA' phonons enhance the phonon scattering.

The shorter phonon lifetimes are due to higher scattering rate, as shown in Fig. 5. Here the three-phonon interaction of absorption (Γ^+: $\lambda + \lambda' \rightarrow \lambda''$) and emission ($\Gamma^-$: $\lambda \rightarrow \lambda' + \lambda''$) processes for flawless Mg_2Si and nanotwinned Mg_2Si are displayed. The peaks in Fig. 5 represent the scattering rate of a phonon with wavelength λ and frequency ω scattered by another phonon with wavelength λ' and frequency ω'. Due to the Mg–Mg pair "rattling" (Fig. 3(f)), nanotwinned Mg_2Si shows much stronger scattering than flawless Mg_2Si in both Γ^+ and Γ^- processes. In the Γ^+ process, the soft and flat LA and TA' phonons (Fig. 3(e)) lead to scattering peaks of nanotwinned Mg_2Si that are much lower than those of Mg_2Si. In the Γ^- process, the high frequency modes of nanotwinned Mg_2Si decompose to low frequency phonons more easily. This shows that the "rattling" can interacts further with the high frequency optical modes, suppressing the heat transport carried by them. Fig. 5 shows clearly that the phonon-phonon interaction in nanotwinned Mg_2Si is much stronger than that of flawless Mg_2Si, another source of lower κ_L in nanotwinned Mg_2Si.

To examine the impact of the phonon mean free paths (MFPs) on κ_L, Fig. 6 displays the cumulative κ_L as a function of MFP in flawless and nanotwinned Mg_2Si at room temperature. The cumulative κ_L shows a crossover at a MFP of 2~3 nm. For the high frequency phonon modes with small MFPs, it is the avoided crossings between LA and optical modes (Fig. 3(b)) that are responsible for the cumulative κ_L of flawless Mg_2Si being lower than that of nanotwinned Mg_2Si. For the low frequency phonon modes with large MFPs, the resonant scattering originating from the Mg–Mg pair "rattling" leads to a much lower cumulative κ_L of nanotwinned Mg_2Si than that of flawless Mg_2Si. At the MFP of ~100 nm, the cumulative κ_L for flawless Mg_2Si is 9.5 W/mK, 80% of the κ_L (11.8 W/mK) for nanotwinned Mg_2Si. This suggests that for effective κ_L reduction, the size of this nanotwin in the Mg_2Si matrix should be controlled to lie between 3 nm and 100 nm.

4. CONCLUSIONS

In Summary, we applied DFT to determine the role of nanotwins on the κ_L of Mg_2Si TE material. We found that the κ_L of nanotwinned Mg_2Si (1.42 and 1.20 $W\,m^{-1}\,K^{-1}$ along the *a* and *c* axis) is decreased 10 fold from that (11.8 $W\,m^{-1}\,K^{-1}$) in single crystalline Mg_2Si. We attribute this κ_L reduction to three aspects:

(i) The weak Mg–Si bond leads to the low phonon velocity in nanotwinned Mg_2Si. In addition, the TB induced lattice mismatch leads to the large anharmonicity.

(ii) The resonant scattering originated from "rattling" of Mg–Mg bond pair leads to soft acoustic and optical modes in nanotwinned Mg_2Si.

(iii) The shorter phonon lifetime and higher scattering rates indicate a stronger phonon-phonon interaction in nanotwinned Mg_2Si.

For the maximum effect in reducing κ_L, the size of this nanotwin Mg_2Si should be controlled to lie between 3 nm and 100 nm in the Mg_2Si matrix.

ACKNOWLEDGEMENTS

This work is partially supported by the 111 Project of China under Project no. B07040. Q.A. and W.A.G were supported by the National Science Foundation CMMI program under grant no. 1727428. S.M. is thankful for the support by Act 211 Government of the Russian Federation, under No. 02.A03.21.0011 and by the Supercomputer Simulation Laboratory of South Ural State University [57].

Supplementary Material: Primitive cell of nanotwinned Mg_2Si after relaxation; Average phonon velocity (v_s), Grüneisen parameter (γ_G) calculation method; Calculated Elastic matrix (C_{ij}) of single crystalline and nanotwinned Mg_2Si.

REFERENCES

[1] G. J. Snyder and E. S. Toberer, Complex thermoelectric materials. Nat. Mater. **7** (2), 105 (2008).

[2] J. He and T. M. Tritt, Advances in thermoelectric materials research: Looking back and moving forward. Science **357**, 1369 (2017).

[3] C. Chang, M. H. Wu, D. S. He, Y. L. Pei, C. F. Wu, X. F. Wu, H. L. Yu, F. Y. Zhu, K. D. Wang, Y. Chen, L. Huang, J. F. Li, J. Q. He, and L. D. Zhao, 3D charge and 2D phonon transports leading to high out-of-plane *ZT* in n-type SnSe crystals. Science **360** (6390), 778 (2018).

[4] T. J. Zhu, Y. T. Liu, C. G. Fu, J. P. Heremans, J. G. Snyder, and X. B. Zhao, Compromise and Synergy in High-Efficiency Thermoelectric Materials. Adv. Mater. **29** (14), 1605884 (2017).

[5] W. G. Zeier, J. Schmitt, G. Hautier, U. Aydemir, Z. M. Gibbs, C. Felser, and G. J. Snyder, Engineering half-Heusler thermoelectric materials using Zintl chemistry. Nat. Rev. Mater. **1** (6), 16032 (2016).

[6] J. W. Zhang, L. R. Song, G. K. H. Madsen, K. F. F. Fischer, W. Q. Zhang, X. Shi, and B. B. Iversen, Designing high-performance layered thermoelectric materials through orbital engineering. Nat. Commun. **7**, 10892 (2016).

[7] G. D. Li, U. Aydemir, M. Wood, W. A. Goddard, P. C. Zhai, Q. J. Zhang, and G. J. Snyder, Defect-Controlled Electronic Structure and Phase Stability in Thermoelectric Skutterudite CoSb3. Chem. Mater. **29** (9), 3999 (2017).

[8] He, J. Q.; Girard, S. N.; Zheng, J. C.; Zhao, L. D.; Kanatzidis, M. G.; Dravid, V. P., Strong Phonon Scattering by Layer Structured PbSnS2 in PbTe Based Thermoelectric Materials. Adv. Mater. **24** (32), 4440 (2012).

[9] Liu, W. S.; Zhang, B. P.; Li, J. F.; Zhao, L. D., Effects of Sb compensation on microstructure, thermoelectric properties and point defect of CoSb3 compound. J. Phys. D: Appl. Phys. **40** (21), 6784 (2007).

[10] He, J. Q.; Blum, I. D.; Wang, H. Q.; Girard, S. N.; Doak, J.; Zhao, L. D.; Zheng, J. C.; Casillas, G.; Wolverton, C.; Jose-Yacaman, M.; Seidman, D. N.; Kanatzidis, M. G.; Dravid, V. P., Morphology Control of Nanostructures: Na-Doped PbTe-PbS System. Nano. Lett. **12** (11), 5979 (2012).

[11] Wu, H. J.; Carrete, J.; Zhang, Z. Y.; Qu, Y. Q.; Shen, X. T.; Wang, Z.; Zhao, L. D.; He, J. Q., Strong enhancement of phonon scattering through nanoscale grains in lead sulfide thermoelectrics. NPG. Asia. Mater. **6**, e108 (2014).

[12] B. A. Xu, T. L. Feng, M. T. Agne, L. Zhou, X. L. Ruan, G. J. Snyder, and Y. Wu, Highly Porous Thermoelectric Nanocomposites with Low Thermal Conductivity and High Figure of Merit from Large-Scale Solution-Synthesized $Bi_2Te_{2.5}Se_{0.5}$ Hollow Nanostructures. Angew. Chem. Int. Edit. **56** (13), 3546 (2017).

[13] Y. Z. Pei, A. D. LaLonde, N. A. Heinz, X. Y. Shi, S. Iwanaga, H. Wang, L. D. Chen, and G. J. Snyder, Stabilizing the Optimal Carrier Concentration for High Thermoelectric Efficiency. Adv. Mater. **23** (47), 5674 (2011).

[14] Goldsmid, H. J. Introduction to Thermoelectricity, Springer, Heidelberg, Germany (2009).

[15] L. D. Hicks and M.S. Dresselhaus, Effect of Quantum-Well Structures on the Thermoelectric Figure of Merit. Phys. Rev. B **47**, 12727 (1993).

[16] L. D. Hicks, T. C. Harman, X. Sun, M. S. Dresselhaus, Experimental study of the effect of quantum-well structures on the thermoelectric figure of merit. Phys. Rev. B **53**, 10493 (1996).

[17] H. S. Kim, N. A. Heinz, Z. M. Gibbs, Y. L. Tang, S. D. Kang, and G. J. Snyder, High thermoelectric performance in $(Bi_{0.25}Sb_{0.75})$(2)Te-3 due to band convergence and improved by carrier concentration control. Mater. Today. **20** (8), 452 (2017).

[18] Y. Z. Pei, X. Y. Shi, A. LaLonde, H. Wang, L. D. Chen, and G. J. Snyder, Convergence of electronic bands for high performance bulk thermoelectrics. Nature **473** (7345), 66 (2011).

[19] Y. L. Tang, Z. M. Gibbs, L. A. Agapito, G. Li, H. S. Kim, M. B. Nardelli, S. Curtarolo, and G. J. Snyder, Convergence of multi-valley bands as the electronic origin of high thermoelectric performance in $CoSb_3$ skutterudites. Nat. Mater. **14** (12), 1223 (2015).

[20] J. P. Heremans, V. Jovovic, E. S. Toberer, A. Saramat, K. Kurosaki, A. Charoenphakdee, S. Yamanaka, and G. J. Snyder, Enhancement of thermoelectric efficiency in PbTe by distortion of the electronic density of states. Science **321** (5888), 554 (2008).

[21] S. Q. Lin, W. Li, Z. W. Chen, J. W. Shen, B. H. Ge, and Y. Z. Pei, Tellurium as a high-performance elemental thermoelectric. Nat. Commun. **7**, 10287(2016).

[22] H. L. Liu, X. Shi, F. F. Xu, L. L. Zhang, W. Q. Zhang, L. D. Chen, Q. Li, C. Uher, T. Day, and G. J. Snyder, Copper ion liquid-like thermoelectrics. Nat. Mater. **11** (5), 422 (2012).

[23] L. D. Zhao, S. H. Lo, Y. S. Zhang, H. Sun, G. J. Tan, C. Uher, C. Wolverton, V. P. Dravid, and M. G. Kanatzidis, Ultralow thermal conductivity and high thermoelectric figure of merit in SnSe crystals. Nature **508** (7496), 373 (2014).

[24] C. W. Li, J. Hong, A. F. May, D. Bansal, S. Chi, T. Hong, G. Ehlers, and O. Delaire, Orbitally driven giant phonon anharmonicity in SnSe. Nature Physics **11** (12), 1063 (2015).

[25] P. J. Ying, X. Li, Y. C. Wang, J. Yang, C. G. Fu, W. Q. Zhang, X. B. Zhao, and T. J. Zhu, Hierarchical Chemical Bonds Contributing to the Intrinsically Low Thermal Conductivity in alpha-MgAgSb Thermoelectric Materials. Adv. Funct. Mater. **27** (1), 1604145 (2017).

[26] X. Y. Zhang, Z. W. Chen, S. Q. Lin, B. Q. Zhou, B. Gao, and Y. Z. Pei, Promising Thermoelectric Ag5-delta Te3 with Intrinsic Low Lattice Thermal Conductivity. ACS. Energy. Lett. **2** (10), 2470 (2017).

[27] W. Li, S. Q. Lin, B. H. Ge, J. Yang, W. Q. Zhang, and Y. Z. Pei, Low Sound Velocity Contributing to the High Thermoelectric Performance of Ag_8SnSe_6. Adv. Sci. **3** (11), 1600196 (2016).

[28] W. Li, L. L. Zheng, B. H. Ge, S. Q. Lin, X. Y. Zhang, Z. W. Chen, Y. J. Chang, and Y. Z. Pei, Promoting SnTe as an Eco-Friendly Solution for p-PbTe Thermoelectric via Band Convergence and Interstitial Defects. Adv. Mater. **29** (17), 1605887 (2017).

[29] L. W. Fu, M. J. Yin, D. Wu, W. Li, D. Feng, L. Huang, and J. Q. He, Large enhancement of thermoelectric properties in n-type PbTe via dual-site point defects. Energ. Environ. Sci. **10** (9), 2030 (2017).

[30] X. Shi, J. Yang, J. R. Salvador, M. F. Chi, J. Y. Cho, H. Wang, S. Q. Bai, J. H. Yang, W. Q. Zhang, and L. D. Chen, Multiple-Filled Skutterudites: High Thermoelectric Figure of Merit through Separately Optimizing Electrical and Thermal Transports. J. Am. Chem. Soc. **133** (20), 7837 (2011).

[31] S. I. Kim, K. H. Lee, H. A. Mun, H. S. Kim, S. W. Hwang, J. W. Roh, D. J. Yang, W. H. Shin, X. S. Li, Y. H. Lee, G. J. Snyder, and S. W. Kim, Dense dislocation arrays embedded in grain boundaries for high-performance bulk thermoelectrics. Science **348** (6230), 109 (2015).

[32] Z. W. Chen, Z. Z. Jian, W. Li, Y. J. Chang, B. H. Ge, R. Hanus, J. Yang, Y. Chen, M. X. Huang, G. J. Snyder, and Y. Z. Pei, Lattice Dislocations Enhancing Thermoelectric PbTe in Addition to Band Convergence. Adv. Mater. **29** (23), 1606768 (2017).

[33] Z. W. Chen, B. H. Ge, W. Li, S. Q. Lin, J. W. Shen, Y. J. Chang, R. Hanus, G. J. Snyder, and Y. Z. Pei, Vacancy-induced dislocations within grains for high-performance PbSe thermoelectrics. Nat. Commun. 8, 13828 (2017).

[34] B. Poudel, Q. Hao, Y. Ma, Y. C. Lan, A. Minnich, B. Yu, X. A. Yan, D. Z. Wang, A. Muto, D. Vashaee, X. Y. Chen, J. M. Liu, M. S. Dresselhaus, G. Chen, and Z. F. Ren, High-thermoelectric performance of nanostructured bismuth antimony telluride bulk alloys. Science **320** (5876), 634 (2008).

[35] Q. H. Zhang, Z. X. Zhou, M. Dylla, M. T. Agne, Y. Z. Pei, L. J. Wang, Y. S. Tang, J. C. Liao, J. Li, S. Q. Bai, W. Jiang, L. D. Chen, and G. J. Snyder, Realizing High-performance Thermoelectric Power Generation through Grain Boundary Engineering of Skutterudite-based Nanocomposites. Nano. Energy **41**, 501 (2017).

[36] X. L. Su, P. Wei, H. Li, W. Liu, Y. G. Yan, P. Li, C. Q. Su, C. J. Xie, W. Y. Zhao, P. C. Zhai, Q. J. Zhang, X. F. Tang, and C. Uher, Multi-Scale Microstructural Thermoelectric Materials: Transport Behavior, Non-Equilibrium Preparation, and Applications. Adv. Mater. **29** (20), 1602013 (2017).

[37] J. Mao, Y. M. Wang, Z. H. Liu, B. H. Ge, and Z. F. Ren, Phonon scattering by nanoscale twin boundaries. Nano. Energy. **32**, 174 (2017).

[38] H. S. Shin, S. G. Jeon, J. Yu, Y. S. Kim, H. M. Park, and J. Y. Song, Twin-driven thermoelectric figure-of-merit enhancement of Bi2Te3 nanowires. Nanoscale. **6** (11), 6158 (2014).

[39] Y. G. Zhou, J. Y. Yang, L. Cheng, and M. Hu, Strong anharmonic phonon scattering induced giant reduction of thermal conductivity in PbTe nanotwin boundary. Phys. Rev. B. **97** (8), 085304 (2018).

[40] J. Tani and H. Kido, Thermoelectric properties of bi-doped Mg2Si semiconductors. Physica. B. **364**, 218, (2005).

[41] G. Kresse and J. Furthmuller, Efficiency of ab-initio total energy calculations for metals and semiconductors using a plane-wave basis set. Comp. Mater. Sci. **6**, 15 (1996).

[42] G. Kresse and J. Furthmuller, Efficient iterative schemes for ab initio total-energy calculations using a plane-wave basis set. Phys. Rev. B. **54**, 11169 (1996).

[43] G. Kresse and D. Joubert, From ultrasoft pseudopotentials to the projector augmented-wave method. Phys. Rev. B. **59**, 1758 (1999).

[44] J. P. Perdew, K. Burke, M. Ernzerhof, Generalized gradient approximation made simple. Phys. Rev. Lett. **77**, 3865 (1996).

[45] A. Togo, F. Oba, I. Tanaka, First-principles calculations of the ferroelastic transition between rutile-type and $CaCl_2$-type SiO_2 at high pressures. Phys. Rev. B. **78**, 134106 (2008).

[46] W. Li, L. Lindsay, D. A. Broido, D. A. Stewart, and N. Mingo, Thermal conductivity of bulk and nanowire Mg2SixSn1-x alloys from first principles. Phys. Rev. B. **86**, 174307 (2012).

[47] W. Li, J. Carrete, N. A. Katcho, and N. Mingo, ShengBTE: A solver of the Boltzmann transport equation for phonons. Comput. Phys. Commun. **185** (6), 1747 (2014).

[48] G. S. Nolas, D. Wang, M. Beekman, Transport properties of polycrystalline Mg2Si1-ySby (0 <= y < 0.4). Phys. Rev. B. **76**, 235204 (2007).

[49] J. I. Jang, J. E. Lee, B. S. Kim, S. D. Park, and H. S. Lee, Twinning and its formation mechanism in a binary Mg2Si thermoelectric material with an anti-fluorite structure. Rsc. Adv. **7** (35), 21671 (2017).

[50] G. D. Li, Q. An, S. I. Morozov, B. Duan, W. A. Goddard, P. C. Zhai, Q. J. Zhang, and G. J. Snyder, Mechanical softening of thermoelectric semiconductor Mg_2Si from nanotwinning. Scripta. Mater. **157**, 90 (2018).

[51] S. P. Green, C. Jones, A. Stasch, Stable magnesium(I) compounds with Mg-Mg bonds. Science **318**, 1754 (2007).

[52] R. S. Busk, Effect of Temperature on the Lattice Parameters of Magnesium Alloys. J. Met. **4**, 207 (1952).

[53] D. H. Chung, Elastic Moduli of Single Crystal and Polycrystalline Mgo.Philos. Mag. **8**, 833 (1963).

[54] T. Caillat, A. Borshchevsky, J. P. Fleurial, Properties of single crystalline semiconducting $CoSb_3$. J. Appl. Phys. **80**, 4442 (1996).

[55] J. G. He, M. Amsler, Y. Xia, S. S. Naghavi, V. I. Hegde, S. Q. Hao, S. Goedecker, V. Ozolins, and C. Wolverton, Ultralow Thermal Conductivity in Full Heusler Semiconductors. Phys. Rev. Lett. **117**, 046602 (2016).

[56] B. L. Huang and M. Kaviany, Filler-reduced phonon conductivity of thermoelectric skutterudites: Ab initio calculations and molecular dynamics simulations. Acta. Mater. **58**, 4516 (2010).

[57] Z. T. Tian, J. Garg, K. Esfarjani, T. Shiga, J. Shiomi, and G. Chen, Phonon conduction in PbSe, PbTe, and $PbTe_{1-x}Se_x$ from first-principles calculations. Phys. Rev. B. **85**, 184303 (2012).

[58] Kostenetskiy, P. S.; and Safonov, A.Y., SUSU Supercomputer Resources. Proceedings of the 10th Annual International Scientific Conference on Parallel Computing Technologies (Arkhangelsk, Russia, 2016).

Table:

Table. 1 Calculated phonon velocities ($v_{LA/TA/TA'}$, v_s), Grüneisen parameter (γ_G), bulk modulus (B), and shear modulus (G) of single crystalline and nanotwinned Mg_2Si, respectively. $v_{LA/TA/TA'}$ is calculated by fitting the slope of the acoustic phonon dispersion around the Γ point. The calculation method for v_s and γ_G are shown in eqn. S1 and S2 in the SM.

System	v_{LA} (m/s)	v_{TA} (m/s)	$v_{TA'}$ (m/s)	v_s (m/s)	γ_G	B (GPa)	G (GPa)
Single crystalline Mg_2Si	7410	4036	3895	4427	1.38	54.6	50.6
Nanotwinned Mg_2Si	6754	3555	3444	3915	1.49	50.6	32.4

Figures:

Figure 1:

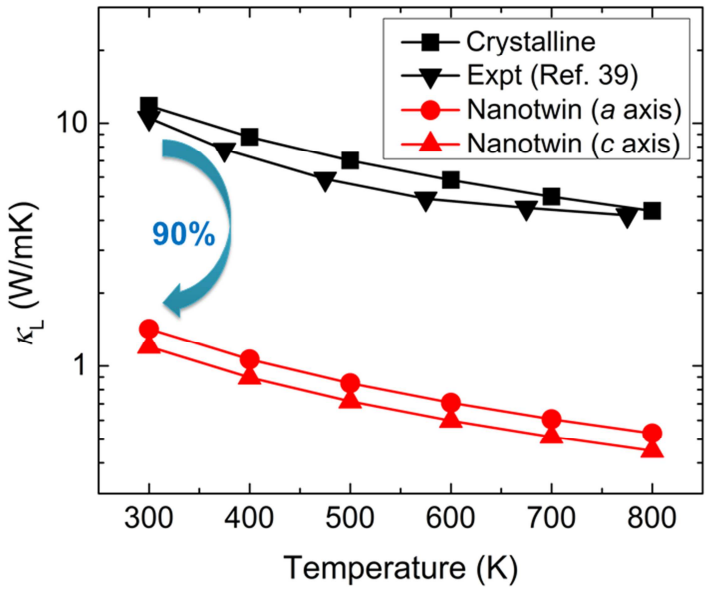

Figure 1. Lattice thermal conductivity (κ_L) of single crystalline and nanotwinned Mg_2Si as a function of temperature, and a comparison with experimental value of bulk Mg_2Si [39].

Figure 2:

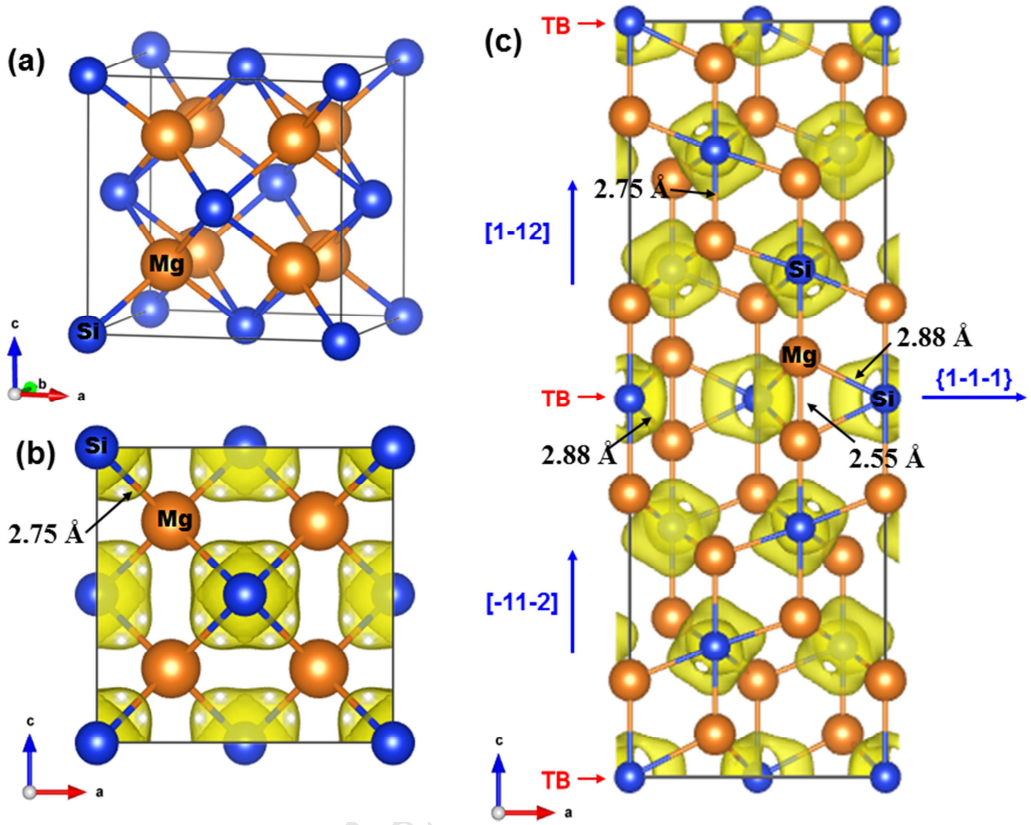

Figure 2. Atomic Structures of single crystalline and nanotwinned Mg_2Si. (a) Crystal structure of single crystalline Mg_2Si showing the FCC unit cell. (b) Atomic structure of Mg_2Si (with calculated isosurfaces at a value of 0.78 of ELF) along the *a*-*c* plane. (c) Atomic structure of nanotwinned Mg_2Si (ELF = 0.78) with the TB along the {1-1-1} plane.

Figure 3:

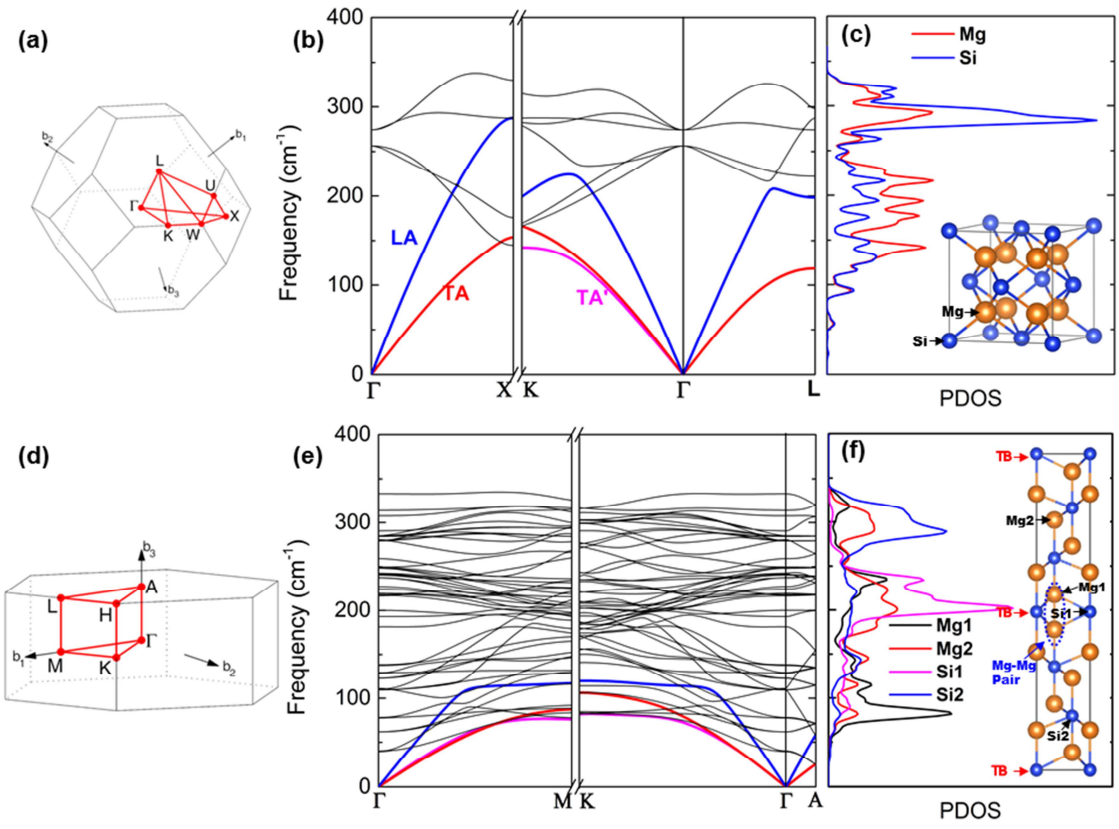

Figure 3. The phonon transport of nanotwinned and flawless Mg_2Si. (a) Brillouin zone and high-symmetry paths in FCC Mg_2Si. (b) Phonon band structures and (c) Phonon density of state (PDOS) of flawless Mg_2Si. (d) Brillouin zone and high-symmetry paths in hexagonal nanotwinned Mg_2Si. (e) Phonon band structures and (f) PDOS of nanotwinned Mg_2Si.

Figure 4:

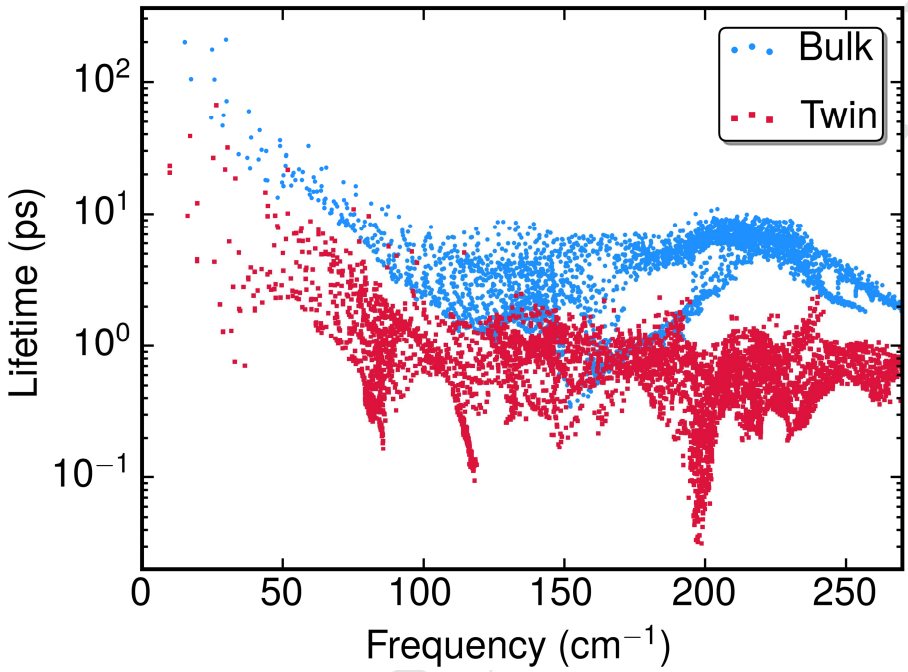

Figure 4. Phonon lifetimes as a function of phonon frequencies for nanotwinned and flawless Mg_2Si at room temperature. This shows that the lifetimes are dramatically lower for the nanotwinned Mg_2Si.

Figure 5:

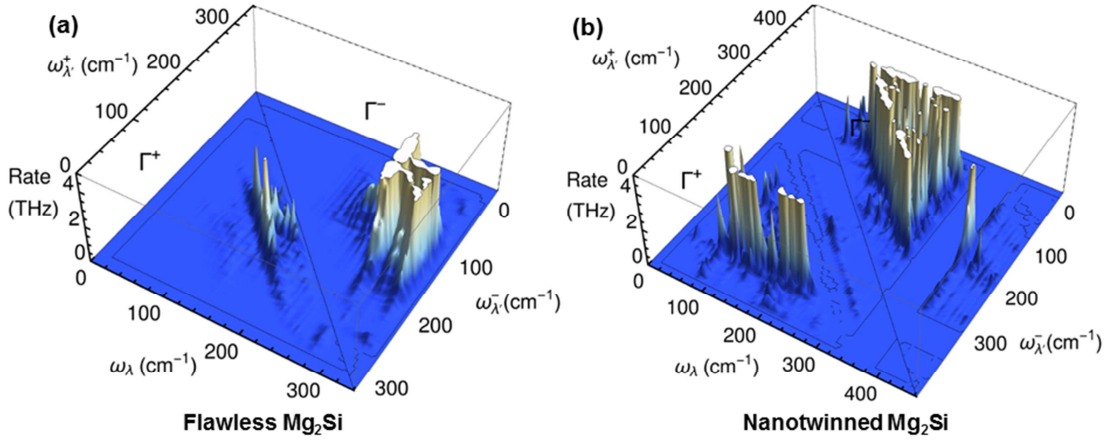

Figure 5. Phonon scattering rates of three-phonon absorption (Γ^{+}) and emission (Γ^{-}) processes for (a) flawless Mg_2Si and (b) nanotwinned Mg_2Si, respectively. This shows that the scattering rates are dramatically faster for the nanotwinned Mg_2Si.

Figure 6:

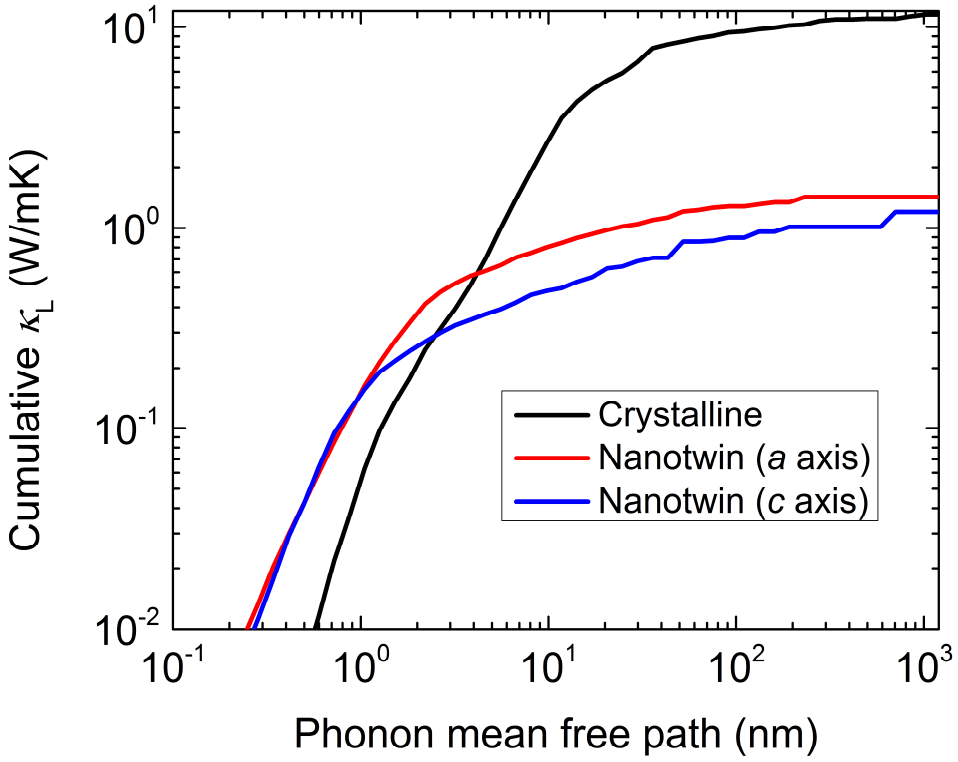

Figure 6. Cumulative contributions to thermal conductivity as a function of phonon MFP at room temperature for flawless and nanotwinned Mg_2Si.

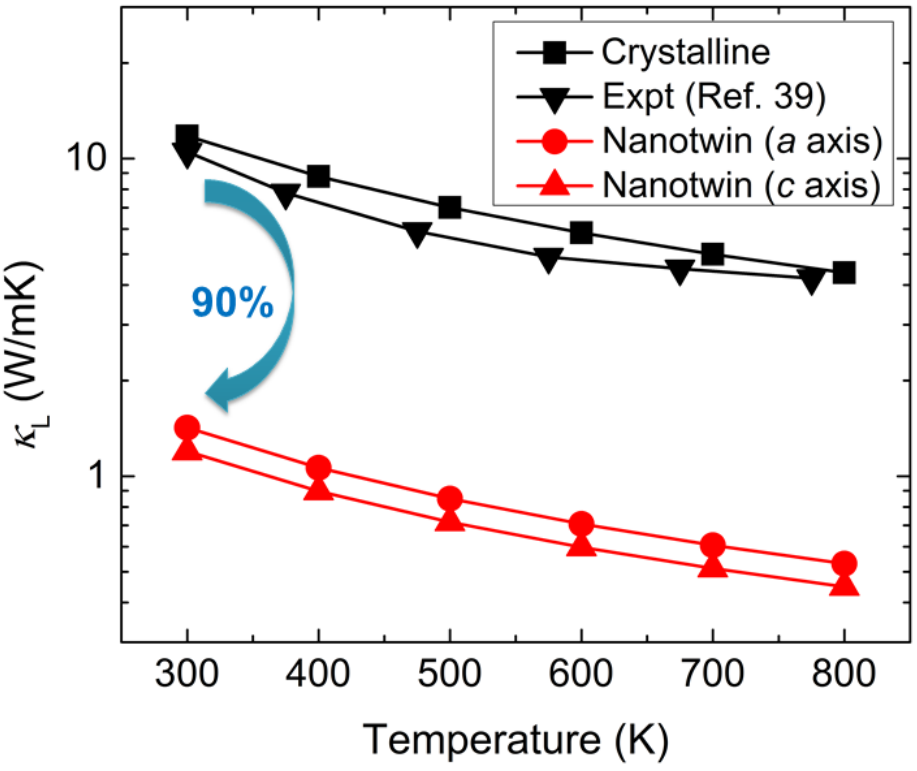
Crystalline
Expt (Ref. 39)
Nanotwin (a axis)
Nanotwin (c axis)
90%
10
1
κ_L (W/mK)
300
400
500
600
700
800
Temperature (K)

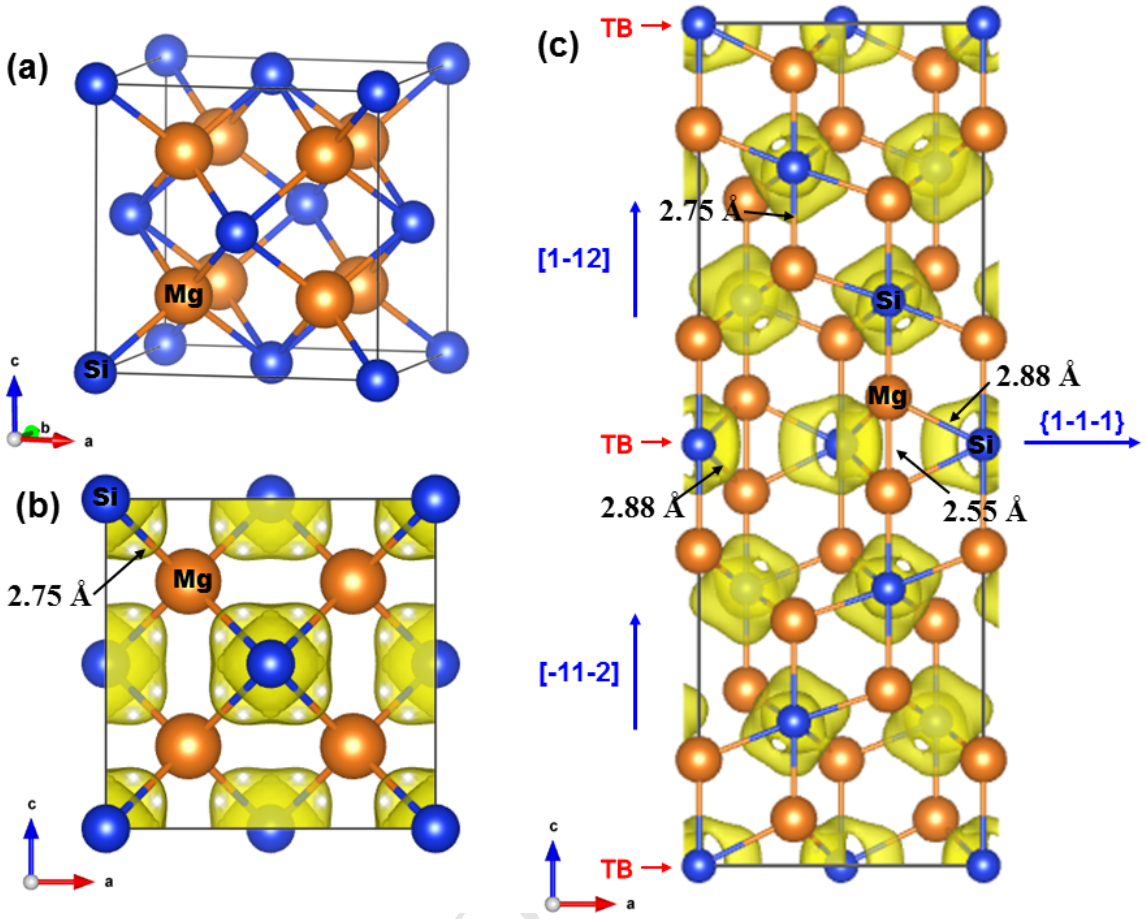
(a)
Mg
Si
c
b
a
(b)
Si
Mg
2.75 Å
c
a
(c)
TB
2.75 Å
[1-12]
Si
Mg
2.88 Å
{1-1-1}
TB
Si
2.88 Å
2.55 Å
[-11-2]
c
TB
a

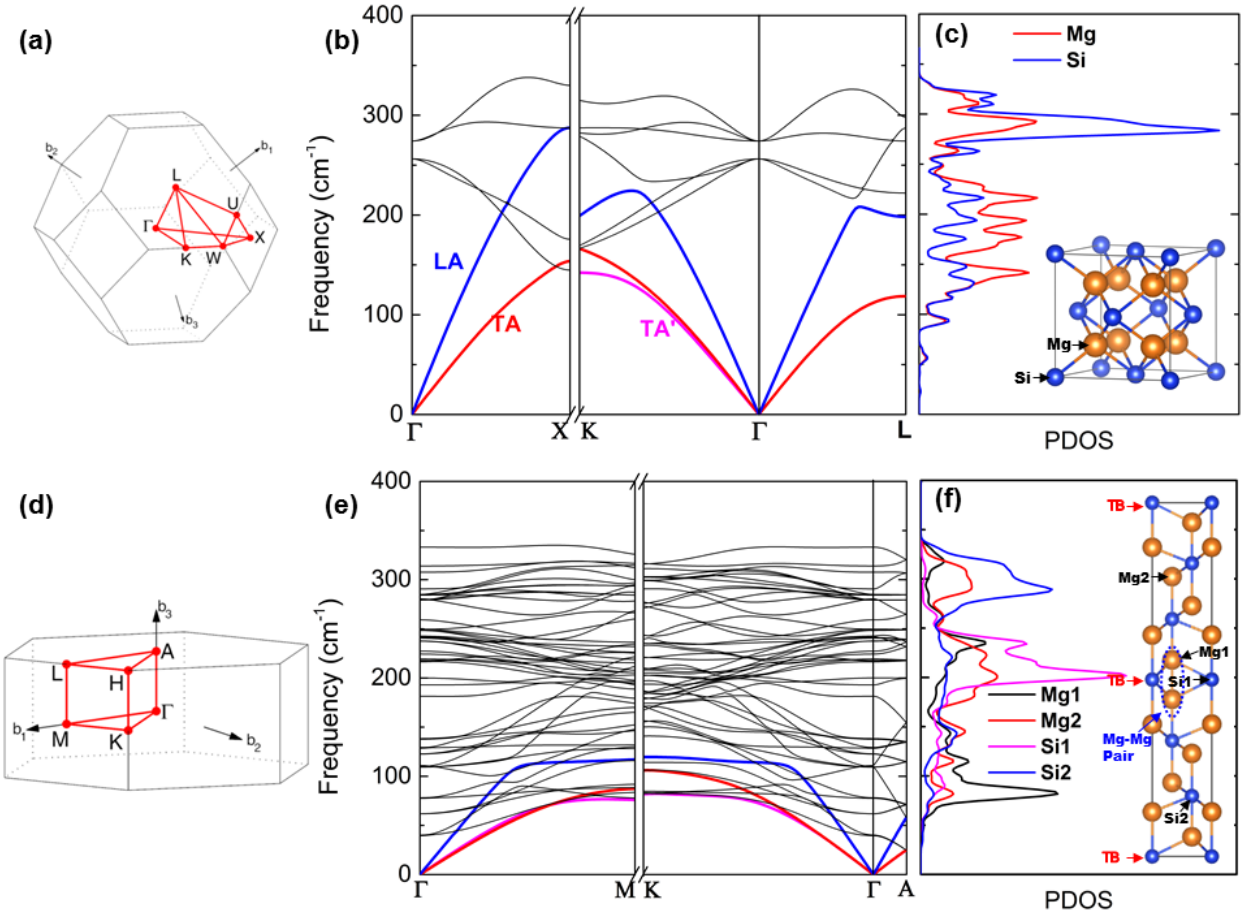
(a)
L
U
Γ
X
K
W
(b)
Frequency (cm-1)
LA
TA
TA'
Γ
X
K
Γ
L
(c)
Mg
Si
Mg
Si
PDOS
(d)
A
L
H
Γ
M
K
(e)
Frequency (cm-1)
Γ
M
K
Γ
A
(f)
TB
Mg2
Mg1
Si1
Mg-Mg Pair
Si2
Mg1
Mg2
Si1
Si2
PDOS

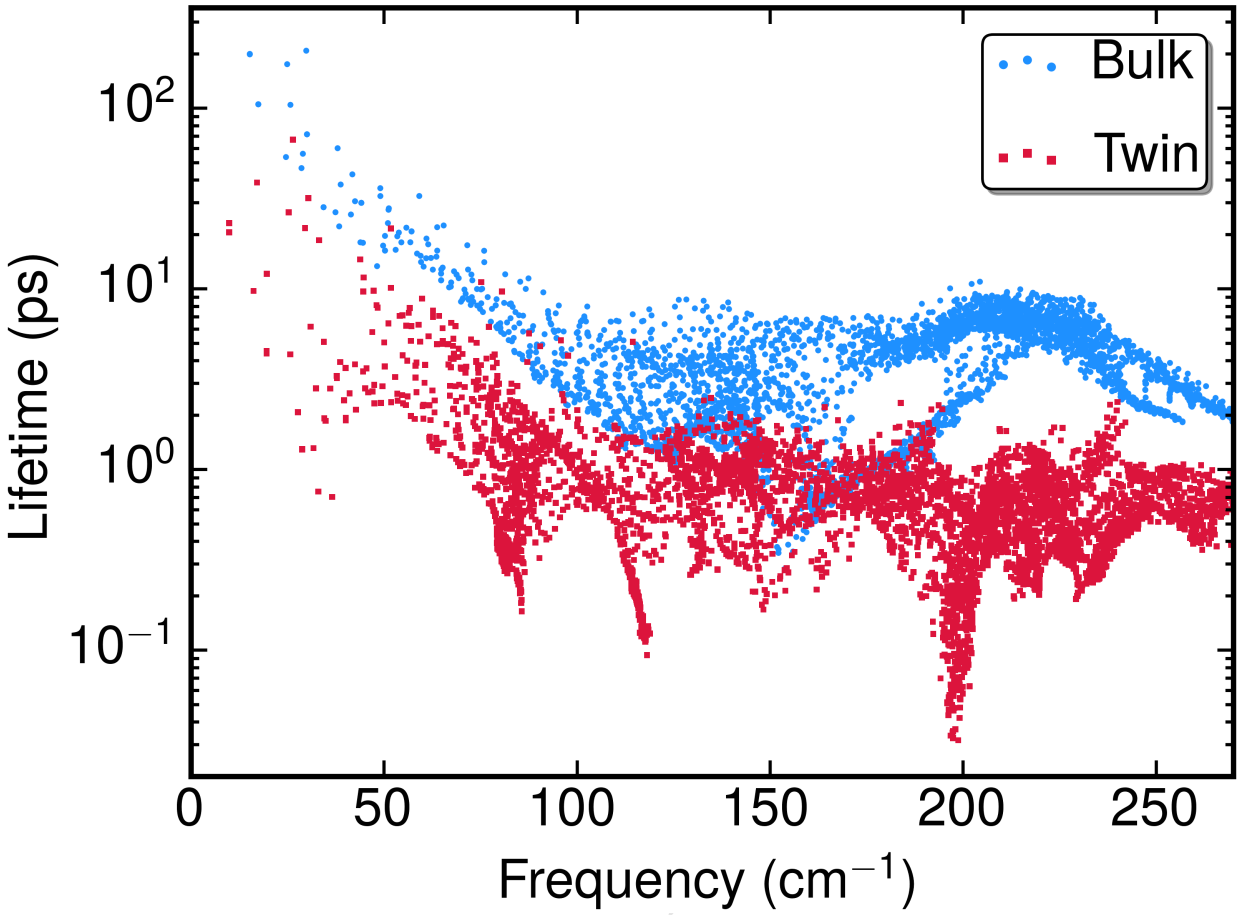

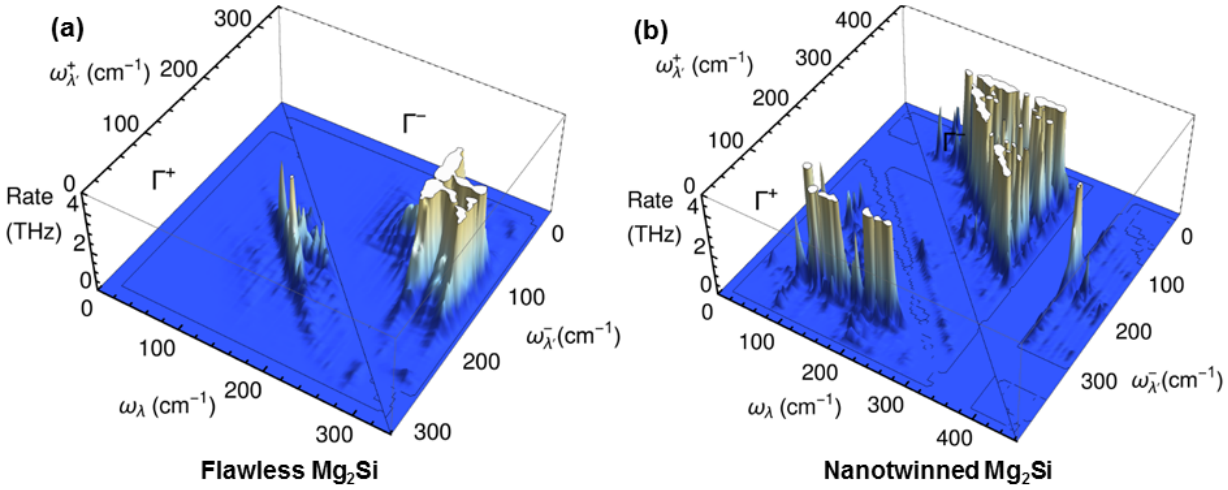
(a)
$\omega^{+}_{\lambda'}$ (cm^{-1})
Rate (THz)
Γ^{+}
Γ^{-}
ω_{λ} (cm^{-1})
$\omega^{-}_{\lambda'}$(cm^{-1})
Flawless Mg_2Si
(b)
$\omega^{+}_{\lambda'}$ (cm^{-1})
Rate (THz)
Γ^{+}
Γ^{-}
ω_{λ} (cm^{-1})
$\omega^{-}_{\lambda'}$(cm^{-1})
Nanotwinned Mg_2Si

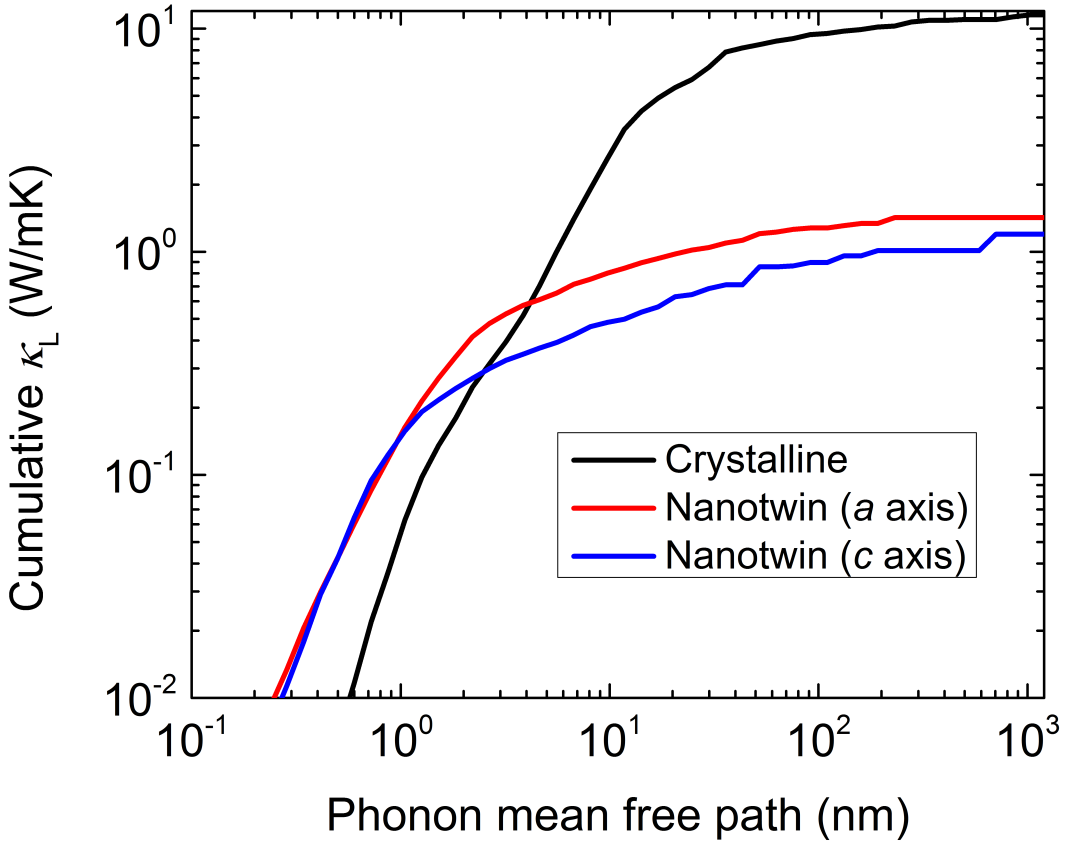
Cumulative κ_L (W/mK)
10^{1}
10^{0}
10^{-1}
10^{-2}
10^{-1}
10^{0}
10^{1}
10^{2}
10^{3}
Phonon mean free path (nm)
Crystalline
Nanotwin (*a* axis)
Nanotwin (*c* axis)

Supplementary Material

Dramatically reduced lattice thermal conductivity of Mg_2Si thermoelectric material from nanotwinning

Guodong Li [a,b], Jiangang He [b], Qi An [c], Sergey I. Morozov [d], Shiqiang Hao [b], Pengcheng Zhai [*,a], Qingjie Zhang [a], William A. Goddard III [e], and G. Jeffrey Snyder [*,b]

[a]Hubei Key Laboratory of Theory and Application of Advanced Materials Mechanics, School of Science, Wuhan University of Technology, Wuhan 430070, China.

[b]Department of Materials Science and Engineering, Northwestern University, Evanston, Illinois 60208, USA.

[c]Department of Chemical and Materials Engineering, University of Nevada Reno, Reno, Nevada 89557, USA

[d]Department of Computer Simulation and Nanotechnology, South Ural State University, Chelyabinsk 454080, Russia

[e]Materials and Process Simulation Center, California Institute of Technology, Pasadena, California 91125, USA.

[*]Corresponding authors: pczhai@126.com; jeff.snyder@northwestern.edu

Primitive cell of nanotwinned Mg_2Si after relaxation

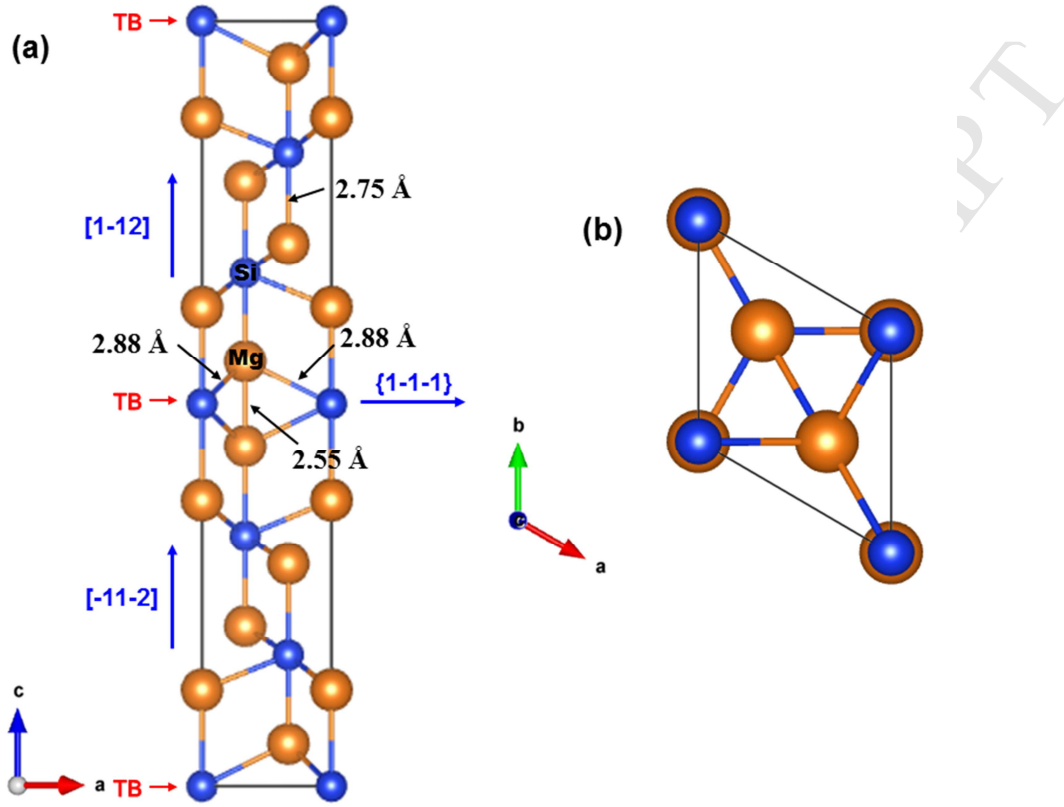

Figure S1. Primitive cell of nanotwinned Mg_2Si along the (a) *a*-*c* plane and (b) *a*-*b* plane, respectively.

Average phonon velocity (v_s), Grueneisen parameter (γ_G) calculation method

The average phonon velocity (v_s) is calculated using the following equation [1]:

$$v_s = \left(\frac{1}{3} \left[\frac{1}{v_{LA}^3} + \frac{1}{v_{TA}^3} + \frac{1}{v_{TA'}^3} \right] \right)^{-1/3} \quad \text{Eqn. S1}$$

where v_{LA}, v_{TA}, $v_{TA'}$ is the three acoustic phonon velocities which is the slope of acoustic phonon dispersions.

The Gruneisen parameter (γ_G) is calculated using the following equation [1]:

$$\gamma_G = \frac{3}{2} \left(\frac{3v_{LA}^2 - 4v_s^2}{v_{LA}^2 + 2v_s^2} \right) \quad \text{Eqn. S2}$$

where v_{LA} and v_s are the LA acoustic phonon velocity and average phonon velocity.

Calculated Elastic matrix (C_{ij}) of single crystalline and nanotwinned Mg_2Si

Table S1. Calculated elastic matrix (C_{ij}) of single crystalline and nanotwinned Mg_2Si. The unit of elastic constants is GPa.

System	C_{11}	C_{12}	C_{13}	C_{22}	C_{23}	C_{33}	C_{44}	C_{55}	C_{66}
Flawless Mg_2Si	117.0	23.45	-	-	-	-	45.37	-	-
Nanotwinned Mg_2Si	88.4	33.4	22.9	-	-	122.2	27.6	26.7	-

REFERENCES:

[1] P. J. Ying, X. Li, Y. C. Wang, J. Yang, C. G. Fu, W. Q. Zhang, X. B. Zhao, and T. J. Zhu, Adv. Funct. Mater. **27** (1), 1604145 (2017).